Effective Hardness of Interaction From Thermodynamics and Viscosity in Dilute Gases

Ian H. Bell[1, a)]
Applied Chemicals and Materials Division, National Institute of Standards and Technology, Boulder, CO 80305

(Dated: 7 April 2020)

The hardness of the effective inverse-power-law potential, which can be obtained from thermodynamics or collision integrals, can be used to demonstrate similarities between thermodynamics and transport properties. This link is investigated for systems of increasing complexity (i.e., the EXP, square-well, Lennard-Jones, and Stockmayer potentials; ab initio results for small molecules; and rigid linear chains of Lennard-Jones sites). These results show that while the two approaches do not yield precisely the same values of effective inverse power law exponent, their qualitative behavior is intriguingly similar, offering a new way of understanding the effective interactions between molecules, especially at high temperatures. In both approaches, the effective hardness is obtained from a double-logarithmic temperature derivative of an effective area.

I. INTRODUCTION

The nature of interactions between chemical entities (atoms, particles, molecules, etc.) underpins all measureable macroscopic thermophysical properties. At all temperatures, measured properties are driven by a delicate equilibrium between attraction and repulsion. At extremely high temperatures, the entities have so much kinetic energy that their interactions are entirely dominated by repulsive interactions; the particles are able to probe increasingly repulsive parts of the potential during the brief time that they are interacting. At lower temperatures, the balance between attraction and repulsion swings in the direction of attraction, and at the Boyle temperature (where the second virial coefficient is zero), the attraction and repulsion balance each other on average.

In the 1960s, significant activity centered around efforts to connect thermodynamic and transport properties of dilute gases[1–8], though that effort seems to have fallen out of favor in the intervening years. This paper aims to nudge the communities of researchers in transport and thermodynamic properties towards each other.

One practical motivation for considering the effective hardness of the interaction is to constrain the functional forms of empirical correlations of thermophysical properties needed for technical applications. It is an unfortunately common situation that no experimental data are available for temperatures much above ambient temperature; this presents obvious problems for applications involving high temperatures, such as combustion. Therefore, developing a theoretically rigorous test for the proper extrapolation of both the virial coefficients and the transport property models at very high temperatures is of great value to ensure that the correct limiting values are reproduced in the limit of infinite temperature, and also that quantitatively correct extrapolation behavior is enforced for high but not infinite temperature.

a)Electronic mail: ian.bell@nist.gov

II. EFFECTIVE IPL EXPONENT

The inverse power law (IPL) potential is given by

$$V = \varepsilon\left(\frac{\sigma}{r}\right)^n \tag{1}$$

with V the potential, ε the energy scaling parameter, σ the length scaling parameter, r the separation, and n the hardness of the repulsion. The second virial coefficient of this potential has a concise closed-form solution[9,10]:

$$B_2 = \frac{2\pi}{3}\sigma^3\Gamma(1-3/n)(T^*)^{-3/n} \tag{2}$$

where $T^* = T/(\varepsilon/k_B)$, and Γ is the mathematical Gamma function.

The IPL satisfies isomorph theory exactly over its entire phase diagram[11] and it is therefore desirable to map the properties of real fluids onto the properties of the IPL. The effective inverse-power-law exponent n_{eff} (sometimes called the density scaling exponent) makes a number of appearances throughout the literature on isomorph theory[12,13]. The quantity n_{eff} arises naturally from the consideration of properties along lines of constant residual entropy, and n_{eff} is used in molecular simulations within isomorph theory to trace out lines of constant residual entropy[13,14] because n_{eff} defines the relationship between temperature and density along a line of constant residual entropy.

Physically, the n_{eff} can be thought of as a means of characterizing how “hard" the interactions are between interacting entities (sites, atoms, molecules). A very large value of n_{eff} indicates that the interactions are more like those of hard spheres (a rigid hard sphere has a n_{eff} of infinity), and the minimum stable IPL potential has an exponent of 3. Strictly speaking, this understanding of the n_{eff} is only valid for fluids for which the correlation between virial energy and potential energy is strong (the necessary condition for the application of isomorph theory), and here the focus is on dilute gases, which, except in the limit of infinite temperature, cannot be expected to necessarily follow isomorph theory. Nevertheless, this parameter still provides useful physical insights.

A. Thermodynamic route

The residual entropy is defined by

$$s^{\mathrm{r}} \equiv s(T,\rho_{\mathrm{N}}) - s^{(\mathrm{ig})}(T,\rho_{\mathrm{N}}) \tag{3}$$

where s is the entropy, $s^{(\mathrm{ig})}$ is the ideal gas entropy, T is the temperature, and ρ_{N} is the number density. The parameter s^+ is then defined by

$$s^+ \equiv \frac{-s^{\mathrm{r}}}{k_{\mathrm{B}}} \tag{4}$$

From thermodynamics, the effective inverse-power-law (IPL) exponent is defined by the thermodynamic relation[15]

$$n_{\mathrm{eff}} \equiv 3\left(\frac{\partial \ln(T)}{\partial \ln(\rho_{\mathrm{N}})}\right)_{s^+} = 3\frac{\rho_{\mathrm{N}}}{T}\left(\frac{\partial T}{\partial \rho_{\mathrm{N}}}\right)_{s^+} \tag{5}$$

It can be obtained directly from an empirical equation of state[16], or from molecular dynamics simulations[17] and is often called the density scaling exponent, in which case the density scaling exponent is given by $n_{\mathrm{eff}}/3$.

Application of the mathematical identity

$$\left(\frac{\partial T}{\partial \rho_{\mathrm{N}}}\right)_{s^+} = -\frac{\left(\frac{\partial s^+}{\partial \rho_{\mathrm{N}}}\right)_T}{\left(\frac{\partial s^+}{\partial T}\right)_{\rho_{\mathrm{N}}}} \tag{6}$$

yields the definition

$$n_{\mathrm{eff}} = -3\frac{\rho_{\mathrm{N}}\left(\frac{\partial s^+}{\partial \rho_{\mathrm{N}}}\right)_T}{T\left(\frac{\partial s^+}{\partial T}\right)_{\rho_{\mathrm{N}}}}, \tag{7}$$

valid for all densities.

In the limit of zero density, $(1/T)\times(\partial s^+/\partial\rho_{\mathrm{N}})_T$ is positive because the entropy of a finite-density gas must always be less than that of an ideal gas at the same temperature and density – interactions, whether attractive or repulsive, increase the structure of the fluid phase. In a virial expansion where virial coefficient terms above B_2 are dropped, the second virial coefficient expansion expression for s^+ is defined by

$$s^+ = \mathfrak{B}_2\rho_{\mathrm{N}} + \dots \tag{8}$$

with the definition

$$\mathfrak{B}_2 \equiv \frac{\mathrm{d}(TB_2)}{\mathrm{d}T} = B_2 + T\frac{\mathrm{d}B_2}{\mathrm{d}T} \tag{9}$$

The zero-density limit of $\rho_{\mathrm{N}}/(\partial s^+/\partial T)_{\rho_{\mathrm{N}}}$ is an indeterminate form of 0/0, therefore, de l'Hôpital's rule yields

$$\lim_{\rho_{\mathrm{N}}\to 0} n_{\mathrm{eff}} = -3\frac{\left(\frac{\partial s^+}{\partial \rho_{\mathrm{N}}}\right)_T}{T}\frac{\cancel{\left(\frac{\partial \rho_{\mathrm{N}}}{\partial \rho_{\mathrm{N}}}\right)_T}^{\,1}}{\left(\frac{\partial^2 s^+}{\partial T\partial \rho_{\mathrm{N}}}\right)_{\rho_{\mathrm{N}}}} \tag{10}$$

and after substitution the result for the effective exponent from thermodynamics is

$$\lim_{\rho_{\mathrm{N}}\to 0} n_{\mathrm{eff}} = -3\frac{T\frac{\mathrm{d}B_2}{\mathrm{d}T} + B_2}{T^2\frac{\mathrm{d}^2B_2}{\mathrm{d}T^2} + 2T\frac{\mathrm{d}B_2}{\mathrm{d}T}} = -\frac{3}{\left(\frac{\mathrm{d}\ln\mathfrak{B}_2}{\mathrm{d}\ln T}\right)} \tag{11}$$

because in the limit of zero density

$$\left(\frac{\partial s^+}{\partial \rho_{\mathrm{N}}}\right)_T = \mathfrak{B}_2 \tag{12}$$

and

$$T\left(\frac{\partial^2 s^+}{\partial T\partial \rho_{\mathrm{N}}}\right) = T^2\frac{\mathrm{d}^2B_2}{\mathrm{d}T^2} + 2T\frac{\mathrm{d}B_2}{\mathrm{d}T} \tag{13}$$

Thus in the zero-density limit, the effective IPL exponent can be obtained directly from the second virial coefficient B_2 and its temperature derivatives. In the case of the IPL potential of hardness n, substitution of Eq. (2) into Eq. (11) yields n again.

Equation (11) can be slightly reformulated to further highlight the similarities with the n_{eff} coming from the viscosity route. To do so, the effective area from the thermodynamic route can be defined as $A_{\mathrm{eff,B_2}} \equiv \mathfrak{B}_2^{2/3}$. Substituting into Eq. (11) yields

$$\lim_{\rho_{\mathrm{N}}\to 0} n_{\mathrm{eff}} = -\frac{3}{\left(\frac{\mathrm{d}\ln A_{\mathrm{eff,B_2}}^{3/2}}{\mathrm{d}\ln T}\right)} = -\frac{2}{\left(\frac{\mathrm{d}\ln A_{\mathrm{eff,B_2}}}{\mathrm{d}\ln T}\right)}. \tag{14}$$

An alternative (defective) definition of the second virial coefficient can be obtained from $n_{\mathrm{eff}} = -3/(\mathrm{d}\ln B_2/\mathrm{d}\ln T)$ in analogy to the viscosity definition of the effective hardness, but this alternative definition is not recommended because the maximum in the second virial coefficient (where $\mathrm{d}B_2/\mathrm{d}T = 0$) results in a pole. A further definition can be obtained from the acoustic virial coefficients (see the SI, Section **??**), but is also not recommended due to the presence of poles. So far, the present definition from Eq. (11), which was obtained rather fortuitously, is the only one that is well-behaved at all temperatures of interest.

B. Viscosity route

To first order in the Sonine expansion, the dilute-gas viscosity of the IPL potential is given by

$$\eta^*_{\rho_{\mathrm{N}}\to 0,\mathrm{IPL}} = \frac{5}{16}\left(\frac{T^*}{\pi}\right)^{1/2}\frac{1}{\Omega^{(2,2)*}} \tag{15}$$

where $\eta^* = \eta\sigma^2/\sqrt{m\varepsilon}$, and with the reduced collision integral $\Omega^{(2,2)*}$ equal to[18] (see supporting information)

$$\Omega^{(2,2)*} = \frac{1}{2}\frac{A_2(\nu = n+1)\Gamma\left(4-\frac{2}{n}\right)}{\left(\frac{2}{n}\right)^{2/n}(T^*)^{2/n}}, \tag{16}$$

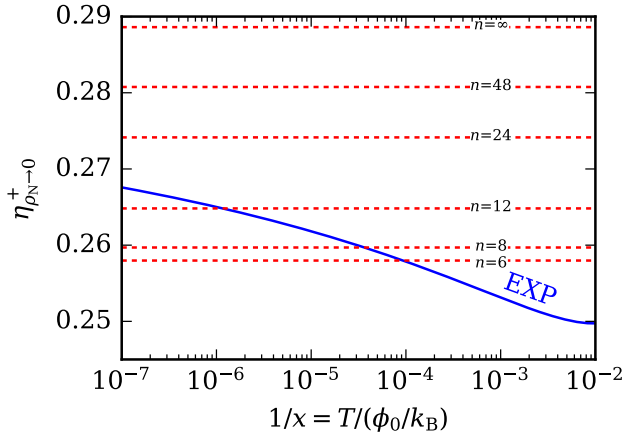

FIG. 1. Values of η^+ for the fully-repulsive IPL potential of hardness n and the EXP potential in the zero-density limit.

where A_2 is a function of the hardness of the potential[18] (see supporting information). Thus in the case of the IPL fluid, $\Omega^{(2,2)*} \propto (T^*)^{-2/n}$. This result, in a different form, was utilized by Hellmann et al. in their discussion of Lennard-Jones chains[19], and in subsequent work on the same theme[20].

If the value of the effective collision integral and its derivative with respect to temperature are imposed to be equal to those of the IPL, an effective hardness can be extracted from the collision integral of the real fluid by the functional form

$$n_{\text{eff}} = \frac{-2\Omega^{(2,2)*}}{T\dfrac{\mathrm{d}\Omega^{(2,2)*}}{\mathrm{d}T}} = -\frac{2}{\left(\dfrac{\mathrm{d}\ln\Omega^{(2,2)*}}{\mathrm{d}\ln T}\right)}. \tag{17}$$

This parameter was explored by Mason[21] in the 1950s for the EXP-6 potential, though a slightly different formulation was used; Mason defined $s_\eta = \ln(\eta)/\ln(T)$, which is related to n_{eff} by $s_\eta = (1/2) + (2/n_{\text{eff}})$. The definition in Eq. (17) is for viscosity, but an analogous formulation can be obtained for self-diffusion from $\Omega^{(1,1)*}$. The formulation in Eq. (17) represents a tautology for the IPL potential. For other potentials, the right-hand-side of Eq. (17) represents the *effective* hardness of the potential obtained from the transport property model. The derivation of this result is in the supporting information (see Section **??**).

As is described in Ref. 18, the value of $\eta^+_{\rho_N\to 0}$ for the IPL fluid has no temperature dependence, only n dependence. Therefore, if the effective inverse power law exponent from transport and thermodynamics both yield approximately the same effective exponent, the value of $\eta^+_{\rho_N\to 0}$ should also approach a value corresponding to the effective IPL exponent. Figure 1 shows the values for selected IPL potentials, and the EXP potential (to be described below). The values are within 10% of the universal value 0.27 proposed by Rosenfeld[22].

C. Entropy Scaling

The framework of modified residual entropy scaling[18,23] provides some guidance on the correct behavior of viscosity models in the dense phase – for fluids that have strong correlations between their virial and potential energies (are strongly correlating in the Roskilde-simple sense), isomorph theory[12,13,15,24–29] describes that the (dimensionless) macroscopically scaled viscosity $\widetilde{\eta}$ should be a monovariate function of the residual entropy over large parts of the phase diagram. Isomorph theory provides a quasi-rigorous explanation for entropy scaling approaches of transport properties. The IPL potential follows entropy scaling exactly, unlike real fluids which can only ever approximate entropy scaling to greater or lesser extents.

The macroscopically reduced viscosity is given by

$$\widetilde{\eta} = \frac{\eta}{\rho_N^{2/3}\sqrt{mk_BT}} \tag{18}$$

where η is the shear viscosity, ρ_N is the number density, m is the mass of one molecule, k_B is Boltzmann's constant, and T is the temperature. Although $\widetilde{\eta}$ diverges at zero number density, when both sides are multiplied by the negative of the residual entropy to the power of 2/3, and a new variable η^+ is defined by

$$\eta^+ \equiv \widetilde{\eta} \times \left(s^+\right)^{2/3} \tag{19}$$

the new term η^+ does not diverge at zero density[18,23]. The zero-density limit of η^+ is given by the form

$$\lim_{\rho_N\to 0}\eta^+ = \frac{\eta_{\rho_N\to 0}}{\sqrt{mk_BT}}(\mathfrak{B}_2)^{2/3} \tag{20}$$

This chimeric formulation includes an effective area coming from viscosity ($\sqrt{mk_BT}/\eta_{\rho_N\to 0}$), and another from thermodynamics ($(\mathfrak{B}_2)^{2/3}$), and therefore the scaled viscosity η^+ is a competition between these two effective areas. The similarity of these areas has been shown in a previous publication[30].

The interest in this scaling, and especially its high-temperature limit, is that the dilute-gas limit of η^+ defines a very narrow band of acceptable values for interactions that can be suitably modeled by an inverse-power-law[18,30] potential of fixed exponent. This had already been shown by Rosenfeld in 1999[22].

D. Repulsion versus attraction

In this section the contributions to the thermodynamic n_{eff} from attractive and repulsive effects are considered individually; such a subdivision cannot be made straightforwardly in the case of transport properties.

The attractive and repulsive contributions cannot be unambiguously decoupled; both have some contribution at all separations (whether that contribution is of import is a separate question). Some historical approaches have focused on splitting the potential into portions where the force ($F = -\mathrm{d}V/\mathrm{d}r$)

is repulsive-only and attractive-only (the Weeks-Chandler-Andersen approach[31]). An alternative approach from Heyes et al.[10] is to consider the contributions to the second virial coefficient from the attractive and repulsive contributions to the residual pressure.

Another means of separating the potential that dovetails with the approach in this paper is to consider the integrand of the virial coefficient defined by

$$B_2 = 2\pi N_A \int_0^\infty [1-\exp(-\beta V(r))] r^2 \mathrm{d}r \tag{21}$$

with $\beta = 1/(kBT)$. At a given temperature, portions of the integrand greater than zero correspond to separations for which the interactions yield positive contributions to B_2 (are repulsive), and integrands less than zero correspond to separations for which the interactions are attractive[32]. If quantum corrections are not included (see below), these contributions correspond to the pairwise separations where the potential is positive or negative. This insight offers a straightforward means to consider independently the attractive and repulsive contributions to the second virial coefficient. The subdivision of the second virial coefficient can be written as

$$B_2 = B_{2,\mathrm{att}} + B_{2,\mathrm{rep}} \tag{22}$$

in which $B_{2,\mathrm{att}}$ is always negative, and $B_{2,\mathrm{rep}}$ is always positive. The effective hardness can be calculated for each contribution by Eq. (11).

Perhaps the simplest prototypical fluid with attraction and repulsion is the square-well fluid defined by

$$V = \begin{cases} \infty & r < \sigma \\ -\varepsilon & \sigma < r < \lambda\sigma \\ 0 & r > \lambda\sigma \end{cases}, \tag{23}$$

which has the virial coefficient contributions (evaluated from Eq. (21) for the negative and positive parts, respectively) of

$$B_{2,\mathrm{rep}} = \frac{2\pi}{3}\sigma^3 \tag{24}$$

$$B_{2,\mathrm{att}} = -\frac{2\pi}{3}\left(\exp(\beta\varepsilon)-1\right)\sigma^3(\lambda^3-1). \tag{25}$$

The value of n_{eff} from the repulsive contribution will always be infinite, but the attractive part has the n_{eff} for $r > \sigma$ of

$$n_{\mathrm{eff,att}} = -3\frac{\exp(\beta\varepsilon)-1-(\beta\varepsilon)\exp(\beta\varepsilon)}{(\beta\varepsilon)^2\exp(\beta\varepsilon)}, \tag{26}$$

where $\beta\varepsilon = 1/T^*$, which is *independent* of the width of the attractive well. The limiting values are 0 for $\beta\varepsilon \to \infty$ and 3/2 for $\beta\varepsilon \to 0$.

The overall reciprocal n_{eff} can be shown (SI, section **??**) to be a weighted average of the reciprocals of the n_{eff} of the attractive and repulsive parts:

$$\frac{1}{n_{\mathrm{eff}}} = \frac{\mathfrak{B}_{\mathrm{rep}}}{\mathfrak{B}_{\mathrm{tot}}}\frac{1}{n_{\mathrm{eff,rep}}} + \frac{\mathfrak{B}_{\mathrm{att}}}{\mathfrak{B}_{\mathrm{tot}}}\frac{1}{n_{\mathrm{eff,att}}} \tag{27}$$

where

$$\mathfrak{B}_\chi = B_\chi + T\frac{\mathrm{d}B_\chi}{\mathrm{d}T}, \tag{28}$$

where the subscript χ indicates the repulsive, attractive, or total contribution.

For the square-well case, the overall n_{eff} therefore reduces to

$$n_{\mathrm{eff,SW}} = \frac{\mathfrak{B}_{\mathrm{tot}}}{\mathfrak{B}_{\mathrm{att}}} n_{\mathrm{eff,att}} \tag{29}$$

E. Summary

The focus of this study is to investigate the behavior of the effective IPL exponent and what lessons this parameter can offer in terms of understanding the nature of interactions between particles and molecules. The focus is on the dilute-gas limit because this limit is analytically accessible; the dilute-gas limit informs the behavior for dense states.

The structure of this paper parallels the analysis in Ref. 30; the effective hardness of the interactions are first investigated for some model fluids in order to obtain insights about the nature of this parameter, and then having a deeper appreciation, these lessons are used to investigate the properties of noble gases and small polyatomic molecules accessible to first principles calculations. The paper closes with a discussion of a practical application of testing the extrapolation of empirical models.

III. MODEL POTENTIALS

Even with advances in the state-of-the-art analysis of molecules from first principles calculations, model potentials still have many lessons to offer because they can be probed to a level of detail that is simply impossible for real substances. Therefore, this section considers some standard pair potentials.

A. Square-Well

The square-well fluid was already discussed above, but here the calculation of its collision integral (and hence its viscosity n_{eff}) is also included. The second virial coefficients of the square-well fluid are particularly concise (see Eq. (24) and Eq. (25)), but the collision integrals are more involved. Modern numerical analysis techniques (adaptive quadrature and Chebyshev expansions) enable accurate calculation of n_{eff} from the viscosity route. The analysis and the Python code are described in the SI.

In the case of the square well fluid (a behavior common to all fluids with an infinitely repulsive hard core), the n_{eff} goes to infinity in the limit of infinite temperature, and in the case of the square well fluid, it also has a pole in its viscosity n_{eff} caused by a maximum in its collision integral, a behavior

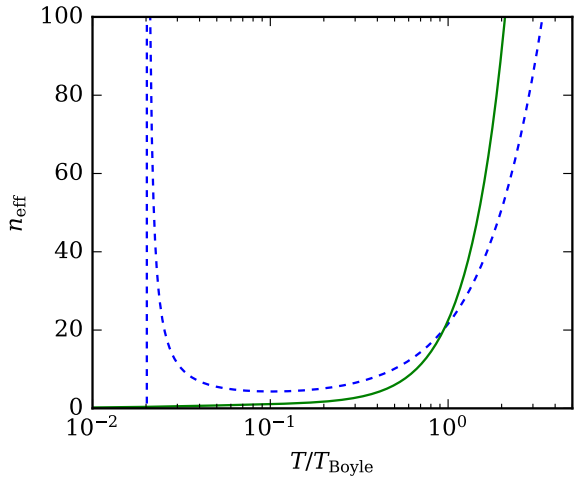

FIG. 2. Values of $n_{\rm eff}$ from the thermodynamic (solid curve) and transport (dashed curve) routes for a square-well potential of $\lambda = 2$

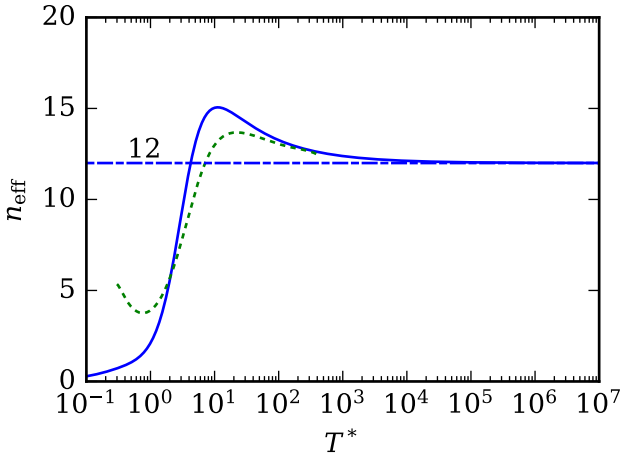

FIG. 3. Effective IPL exponent $n_{\rm eff}$ for the Lennard-Jones 12-6 potential from the B_2 formulation of Jones[33–35] (solid curve) and from the empirical collision integral correlation from Kim and Monroe[36] (dashed curve)

that seems to be consistent with molecular fluids (see below), though none of the ab initio calculations extend to temperatures low enough to definitively locate the maximum of the collision integral.

B. Lennard-Jones

The second virial coefficients of the Lennard-Jones fluid are known exactly from closed-form expressions. In addition, the Lennard-Jones fluid is frequently considered as the reference fluid for estimating dilute-gas transport properties, so it is important to see how well (or not) this model captures the correct behavior of real fluids.

A number of closed-form solutions for the second virial coefficient B_2 of the Lennard-Jones fluid are available in the literature, but a convenient formulation is that of Jones[33] (of Lennard-Jones fame), and recently re-presented by Sadus[34,35], given for the general Mie potential

$$V = \varepsilon \left(\frac{n}{n-m}\right)\left(\frac{n}{m}\right)^{m/(n-m)}\left[\left(\frac{\sigma}{r}\right)^n - \left(\frac{\sigma}{r}\right)^m\right] \tag{30}$$

by

$$B_2^* = \frac{B_2}{\sigma^3} = \frac{2}{3}\pi F(y) \tag{31}$$

with

$$y^n = \left(\frac{n}{n-m}\right)^n \left(\frac{n-m}{m}\right)^m (T^*)^{m-n} \tag{32}$$

and

$$\frac{F(y)}{y^{\frac{3}{(n-m)}}} = \left\{\Gamma\left(\frac{n-3}{n}\right) - \frac{3}{n}\sum_{i=1}^{\infty}\Gamma\left(\frac{im-3}{n}\right)\frac{y^i}{i!}\right\} \tag{33}$$

While Eq. (33) contains an infinite sum, the series is convergent, and 200 terms were used, ensuring a very accurate formulation. Figure 3 presents values for the effective IPL exponent calculated from Eq. (31) in concert with Eq. (11), which yields a value for the effective IPL exponent equal to zero approaching zero temperature, and after passing through a maximum, approaches the asymptote of an effective IPL exponent of 12 at high temperatures. The high-temperature limit captures the repulsive part of the pairwise interactions, and accordingly, for the Mie potential, the high-temperature limit for the IPL exponent is equal to the exponent n in Eq. (30).

To first order in the Sonine expansion, the dilute-gas viscosity formulation for the Lennard-Jones fluid is given by

$$\eta^*_{\rho_{\rm N}\to 0} = \frac{5}{16}\sqrt{\frac{T^*}{\pi}}\frac{1}{\Omega^{(2,2)*}} \tag{34}$$

where the collision integral $\Omega^{(2,2)*}$ is as given by the empirical form of Kim and Monroe[36], and η^* is defined in the same manner as the IPL potential. Higher-order correction terms are not used here in order to ensure consistency with the dilute-gas viscosity of the IPL potential. The value of η^+ is then obtained from

$$\eta^+ = \frac{\eta^*}{\sqrt{T^*}}(\mathfrak{B}_2^*)^{2/3}, \tag{35}$$

where $\mathfrak{B}_2^* = B_2^* + T^* {\rm d}B^*/{\rm d}T^*$ is obtained from analytic derivatives of B_2^*.

Figure 4 shows the calculated values of η^+ in the domain of validity of the correlation of Kim and Monroe[36] ($0.3 \le T^* \le 400$). The curve approaches the value of 0.264822 at high temperatures (the value for an IPL exponent of 12; see the SI of Ref. 30). The extrapolation behavior for $T^* > 400$ of the collision integral correlation of Kim and Monroe is incorrect (See the SI of Ref. 18); the collision integral should approach the behavior of an IPL of exponent $n = 12$.

The effective IPL exponent for viscosity can be obtained by evaluation of Eq. (17) for the Lennard-Jones fluid. An empirical equation for the collision integral $\Omega^{(2,2)*}$ is provided in

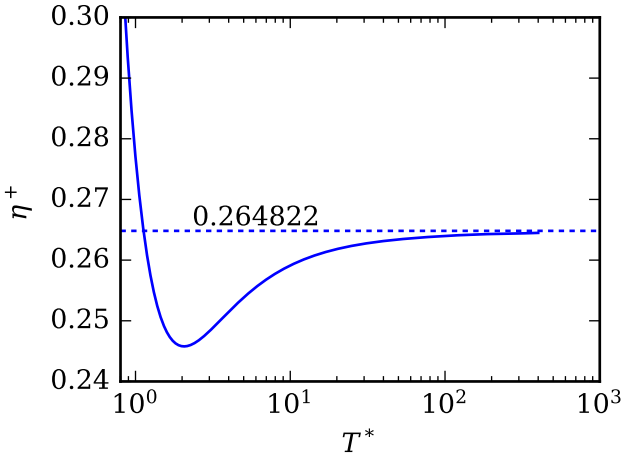

FIG. 4. Dilute values of η^+ for the Lennard-Jones 12-6 potential

the work of Kim and Monroe[36], and complex step derivatives are used to evaluate the temperature derivative with minimal loss in precision. Figure 3 also shows calculated values for the effective IPL exponent in the domain of validity of the correlation. At high temperatures, there is spurious curvature in the function caused by the empirical fit, but the effective hardness of the potential is approaching the curve for the thermodynamic effective hardness.

The Lennard-Jones fluid is a demonstration of excellent consistency between the high-temperature behavior of its thermodynamic and transport models – both approach the behavior of $n_{\text{eff}} = 12$ at high temperatures.

C. EXP

As will be evident from a consideration of the noble gases, the Lennard-Jones fluid does not share its repulsive behavior with the noble gases. A pair potential that more faithfully captures the high-temperature behavior is the EXP potential, which is defined by

$$V = \phi_0 \exp(-r/r_0), \tag{36}$$

where ϕ_0 is the energy scaling parameter, and r_0 is the length scaling parameter.

Sherwood and Mason give the approximate second virial cofficient of this potential by[37]

$$B_2 = \frac{2\pi}{3} r_0^3 \widetilde{B}, \tag{37}$$

where the dimensionless quantity $\widetilde{B}$ is given by

$$\widetilde{B} = \ln(\gamma x)^3 + c_1 \ln(\gamma x) + c_2 + \frac{6\exp(-x)}{x^3} + \ldots, \tag{38}$$

where $c_1 = 4.93480199414941$, $c_2 = 2.40411445241682$, and $\gamma = 1.781072417990198$, and where the dots signify higher-order terms that are dropped (see Ref. 30 and its supporting information). With the definition $x = \phi_0/(k_B T)$, $\mathrm{d}x/\mathrm{d}T = -x/T$,

$$T\frac{\mathrm{d}\widetilde{B}}{\mathrm{d}T} = -x\frac{\mathrm{d}\widetilde{B}}{\mathrm{d}x}, \tag{39}$$

and therefore

$$\mathfrak{B}_2 = \frac{2\pi}{3} r_0^3 \left(\widetilde{B} - x\frac{\mathrm{d}\widetilde{B}}{\mathrm{d}x}\right). \tag{40}$$

The x derivative term is given by

$$-x\frac{\mathrm{d}\widetilde{B}}{\mathrm{d}x} = -3\ln(\gamma x)^2 - c_1 + \exp(-x)\left(\frac{6}{x^2} + \frac{18}{x^3}\right). \tag{41}$$

In order to evaluate n_{eff}, the second derivative term is needed

$$T^2\frac{\mathrm{d}^2\widetilde{B}}{\mathrm{d}T^2} = x^2\frac{\mathrm{d}^2\widetilde{B}}{\mathrm{d}x^2} + 2x\frac{\mathrm{d}\widetilde{B}}{\mathrm{d}x}, \tag{42}$$

and the second derivative with x as the independent variable is

$$\begin{aligned} x^2\frac{\mathrm{d}^2\widetilde{B}}{\mathrm{d}x^2} = \{&-c_1 - 3\ln(\gamma x)^2 + 6\ln(\gamma x) \\ &+ \exp(-x)\left(\frac{6}{x} + \frac{36}{x^2} + \frac{72}{x^3}\right)\} \end{aligned} \tag{43}$$

After substitution into Eq. (11) and cancellation

$$n_{\text{eff}} = -3\frac{\widetilde{B} - x\dfrac{\mathrm{d}\widetilde{B}}{\mathrm{d}x}}{x^2\dfrac{\mathrm{d}^2\widetilde{B}}{\mathrm{d}x^2}} \tag{44}$$

which yields the curve in Fig. 5, which is a monovariate function of the parameter x. The curve is nearly linear in these semi-log coordinates, except for at very high temperatures where a very subtle deviation from linearity is present.

The values of ϕ_0/k_B are on the order of 5×10^7 K for noble gases (see the SI of Ref. 30), therefore, even though Eq. (44) has a pole at $1/x \approxeq 0.474$, the range of applicability of the EXP potential is up to approximately 10^7 K, well above the temperature that atoms are ionized. For instance, the first ionization limit (temperature at which 1% of atoms are ionized) for the noble gases from helium to xenon are on the order of 10^3 K[38], a factor of 10^4 smaller than the approximate limit of the EXP model.

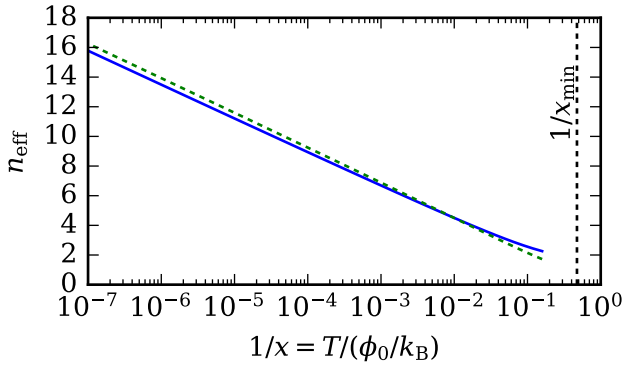

FIG. 5. Effective IPL exponent $n_{\rm eff}$ for the EXP potential from thermodynamics (solid curve) and viscosity (dashed curve, from Eq. (46))

The collision integral of the EXP potential is available in tabular form[39], so to make use of it, an empirical equation was fit in order to evaluate Eq. (17) in a manner analogous to that of the Lennard-Jones 12-6 potential. In previous work[18], no derivatives of the collision integral were needed, and interpolation was used, but a different approach is required here. A rational polynomial function of the form

$$I_{22} = \frac{\sum_i n_i \alpha^i}{\sum_i d_i \alpha^i}, \tag{45}$$

where $\alpha = \ln(x)$, was fit to the tabulated data of I_{22} from Ref. 39 with the use of unweighted differential evolution minimization of the sum of square deviations with all coefficients $\vec{n}$, $\vec{d}$ constrained to be in (-1000, 1000), and $d_0 = 1$. Plots of this function and the fitted values are in the SI (see section **??**). The effective collision integral is defined by $\widetilde{\Omega}_{22} = \alpha^2 I_{22}$. The derivative in Eq. (17) is therefore expressed as

$$T\frac{\mathrm{d}\widetilde{\Omega}_{22}}{\mathrm{d}T} = T\frac{\mathrm{d}\widetilde{\Omega}_{22}}{\mathrm{d}\alpha}\frac{\mathrm{d}\alpha}{\mathrm{d}x}\frac{\mathrm{d}x}{\mathrm{d}T} = -\frac{\mathrm{d}\widetilde{\Omega}_{22}}{\mathrm{d}\alpha}, \tag{46}$$

and evaluated through the use of complex step derivatives. The values of $n_{\rm eff}$ coming from the viscosity model are shown in Fig. 5, showing a striking similarity to those of the thermodynamic model.

D. Stockmayer

The canonical 12-6-3 Stockmayer pair potential is the Lennard-Jones 12-6 potential with the subtraction of an orientation-dependent point dipole contribution,

$$V(r,\theta_1,\theta_2,\phi) = 4\varepsilon\left[\left(\frac{\sigma}{r}\right)^{12} - \left(\frac{\sigma}{r}\right)^{6}\right] - V_\mu \tag{47}$$

where

$$\frac{V_\mu}{\varepsilon(\mu^*)^2\left(\frac{\sigma}{r}\right)^3} = [2\cos\theta_1\cos\theta_2 - \sin\theta_1\sin\theta_2\cos\phi] \tag{48}$$

This potential is a commonly considered model for species with dipolar interactions[40].

Definition of the reduced dipole moment $(\mu^*)^2$ and description of calculation of B_2 from the closed form solution of Bartke and Hentschke[41] (with additional terms in the series expansion) are described in detail in Ref. 30 (and its SI). These terms are needed to calculate $n_{\rm eff}$ from the thermodynamic route. Multicomplex derivatives from the `pymcx` Python package[42] are used to calculate the temperature derivatives. Figure 6 shows the results of these calculations for the thermodynamic $n_{\rm eff}$, for which a coherent result is seen: the stronger the relative strength of the dipole, the more the peak value of $n_{\rm eff}$ is reduced. The curves are obtained from analytic solutions and are smooth. Even for very large dipole moments, the qualitative behavior of $n_{\rm eff}$ doesn't change significantly (the value for $(\mu^*)^2$ for ordinary water is on the order of five[43] (pp. 599)). In this case, scaling the temperatures by the Boyle temperature does not cause collapse of the $n_{\rm eff}$ coming from the thermodynamic route.

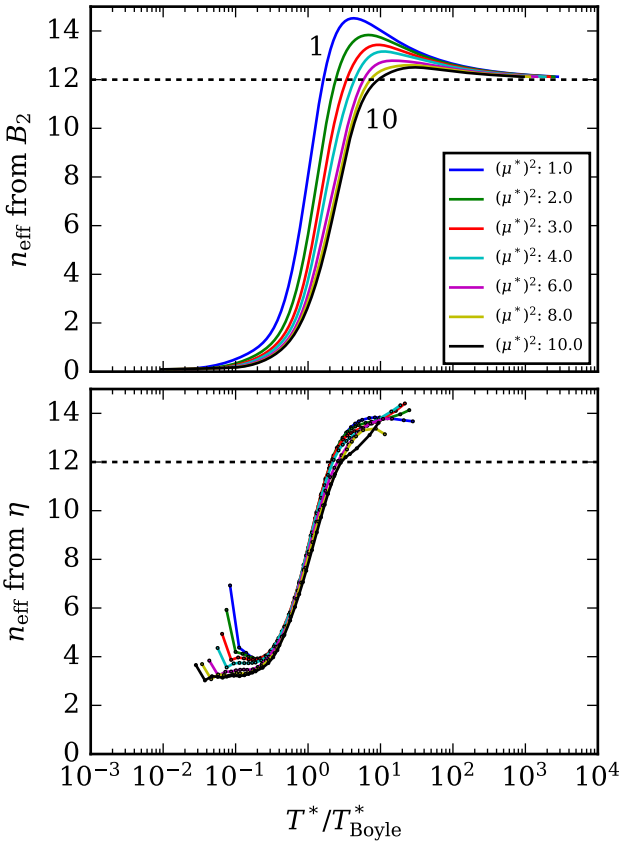

FIG. 6. Values for $n_{\rm eff}$ from thermodynamic and transport routes for the Stockmayer potentials with $(\mu^*)^2 = (1,2,3,4,6,8,10)$.

For the viscosity route for $n_{\rm eff}$, tabulated values of the collision integral are available in Monchick and Mason[44] for values of $(\mu^*)^2 = (1,2,3,4,6,8,10)$; Smith and Munn[45] identify issues with the collision integrals for $T^* > 30$, so skepticism of the high-temperature behavior is appropriate. In order to evaluate the temperature derivative of the collision integral, a

two-fold approach was taken:

- the data points for the Stockmayer fluid of dipole $(\mu^*)^2$ were divided by the values for the Lennard-Jones fluid at the same value of T^*. This is notionally the same approach taken by Xiang et al.[40].
- an interpolating spline function (without any smoothing) was used to fit the reduced collision integral with the `splrep` function of `scipy.interpolate`. The temperature derivative of this functional form was then employed to calculate n_{eff} from Eq. (17).

While there is still some irregularity in these curves caused by the collision integral data, over almost an order of magnitude in temperature, the collapse of the n_{eff} curves is nearly complete when the temperature is scaled by the Boyle temperature. The high-temperature limit must be a n_{eff} of 12, as the repulsive exponent dominates the high-temperature behavior, so all other behaviors seen here can be ascribed to noise in the collision integral data; the present data do not permit a conclusive discussion of the correct high temperature behavior for polar fluids. At low temperatures, the n_{eff} increases again, similar to the case of the Lennard-Jones fluid. The larger $(\mu^*)^2$ is, the lower the minimum of the viscosity n_{eff} is; this partly helps to explain the results for water shown below.

IV. AB INITIO

In recent years, first principles (ab initio) calculations of thermophysical properties of dilute gases have become tractable for small rigid molecules, and these results form the basis of this section.

A. Atomic

In the case of the noble gases, ab initio calculations of the virial coefficients and transport properties are available. Reference 30 collected the recommended ab initio data that existed as of that publication in tabular form.

1. *Pair Potentials*

Before considering the thermophysical properties of the noble gases in the dilute gas limit, it is instructive to consider their pair potentials as calculated from ab initio calculations. Figure 7 shows the ab initio calculated potentials for the noble gases taken from the literature. If the natural logarithm of both sides of Eq. (36) is taken, the equation can be rewritten as

$$\ln(V/k_{\text{B}}) = \ln(\phi_0/k_{\text{B}}) - r/r_0, \tag{49}$$

therefore if the pair potential V approaches a linear curve in $\ln(V)$ versus r coordinates, the pair potential is approaching an EXP potential. This figure demonstrates that the repulsive core of the noble gases are indeed fairly modeled by the EXP potential because their smallest separations correspond to approximately linear curves in these semi-logarithmic coordinates. The assumption of exponential repulsion in the repulsive core was used directly for argon[46] and krypton[47] when fitting their empirical potential functions. The behavior of an exponential repulsion is contrary to the commonly assumed repulsion of IPL of fixed exponent (e.g., in the Lennard-Jones 12-6 potential); when taking the logarithms of both sides of Eq. (1), the result is $\ln(V) = \ln(\varepsilon\sigma^n) + n\ln(r)$, a linear dependence on $\ln(r)$, which is decidedly not the behavior shown in the figure at small separations. That is to say, the repulsion of the Lennard-Jones fluids is too steep and the repulsion should be exponential rather than inverse-power, a result that has been previously described (e.g., see Ref. 48 or Fig. 6. from Ref. 49).

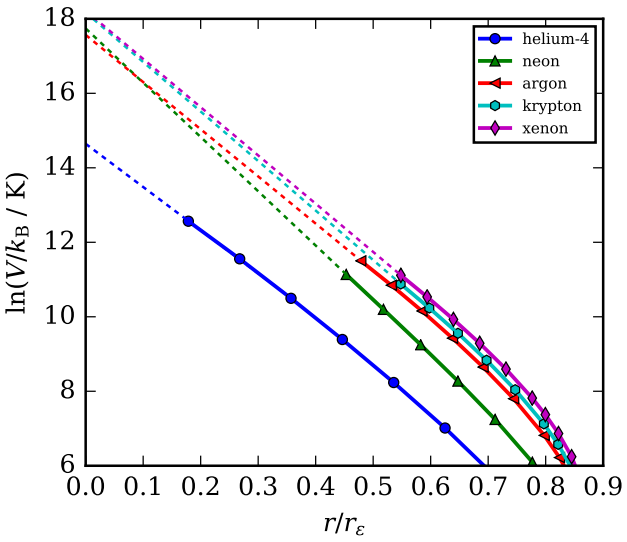

FIG. 7. Pair potential calculated from ab initio methods for the noble gases from the literature (helium-4[50], neon[51], argon[52], krypton[47], xenon[53]), with markers at each tabulated potential value connected with straight line segments, and with pair separation r normalized by the pair separation at the minimum of the potential. The dashed lines show extrapolation to zero separation.

2. *Virial Coefficients*

In Ref. 30, empirical correlations of second virial coefficients were developed in order to evaluate their temperature derivatives. While these correlations were generally adequate for evaluation of first derivatives of B_2[30], the requirement of also yielding correct second temperature derivatives of B_2 does not always apply. Therefore, a more accurate method for calculation of virial coefficient models was required in this work. It is well known in the numerical analysis literature that taking derivatives of noisy data is problematic, and it proved very challenging to obtain reliable values of n_{eff} from fits of ab initio virial coefficient data due to the necessity of having

accurate second derivatives with respect to temperature.

By far the most robust solution for the noble gases proved to be the integration of the empirical Tang-Toennies potentials for each species. The Tang-Toennies empirical fit to the potential is given by

$$V(R) = A\exp(a_1 R + a_2 R^2 + a_{-1}R^{-1} + a_{-2}R^{-2}) - \sum_{n=3}^{8} \frac{C_{2n}}{R^{2n}} \left[1 - \exp(-bR) \sum_{k=0}^{2n} \frac{(bR)^k}{k!}\right] \quad (50)$$

and the necessary coefficients are given in each respective publication (neon[54], argon[46], krypton[47], xenon[53]), and provided in the SI. The second virial coefficients are obtained by a third-order quantum correction, as is described in detail in the supporting information (see the SI, section **??**). The second virial coefficient is then obtained from

$$B_2 = B_{\mathrm{cl}}(T) + \lambda B_{\mathrm{qm},1}(T) + \lambda^2 B_{\mathrm{qm},2}(T) + \lambda^3 B_{\mathrm{qm},3}(T) \quad (51)$$

with $\lambda = \hbar^2/(12mk_{\mathrm{B}}T)$, where m is the mass of one atom in kg, k_{B} is Boltzmann's constant (1.380649×10^{-23} J K^{-1}), and $\hbar = 1.054571817 \times 10^{-34}$ J s. The classical term reads

$$B_{\mathrm{cl}} = -2\pi N_{\mathrm{A}} \int_0^\infty [\exp(-\beta V) - 1] r^2 \mathrm{d}r \quad (52)$$

and the higher order quantum terms are of a similar form, but with different integrands.

Each of the contributions in Eq. (51) are indefinite integrals (see for instance the description in Ref. 55). The repulsive core of these potentials were "patched" with the exponential core with the curves provided in the literature, and supplemented in this work with curves for the fluids (neon, xenon) where none was provided previously. The integrals were joined into a single integral, and integrated from $0.01R_\varepsilon$ to $100R_\varepsilon$ with trapezoidal integration, where R_ε is the separation at the minimum of the potential. Multicomplex algebra from the `pymcx` package[42] in Python was used to obtain numerical derivatives of B_2 with respect to temperature with accuracy approaching numerical precision. This approach yields values of B_2 and its temperature derivatives, the ingredients needed to evaluate n_{eff}.

In the case of helium-4, calculations of the virial coefficients (and n_{eff}) were taken from fully quantum calculations obtained from the literature[56]. The resulting values of n_{eff} are calculated for temperatures from 1 K to 10,000 K, and no additional analysis was needed in order to obtain values for n_{eff}. Figure 8 shows the values obtained from the ab initio calculations, showing a somewhat similar qualitative behavior to Fig. 3, albeit with a much larger magnitude peak. The theory behind n_{eff} was primarily developed for the liquid phase, and the explanation for the large magnitude of the peak is not presently clear. One possible explanation is that the helium atom is somewhat more delocalized as quantum effects become more important, and the probability of finding a helium-4 atom in the repulsive well of the potential becomes more likely than would otherwise be expected. It should be noted that an even more accurate potential is now available for helium-4[57], but that potential has not yet been used to calculate collision integrals or virial coefficients.

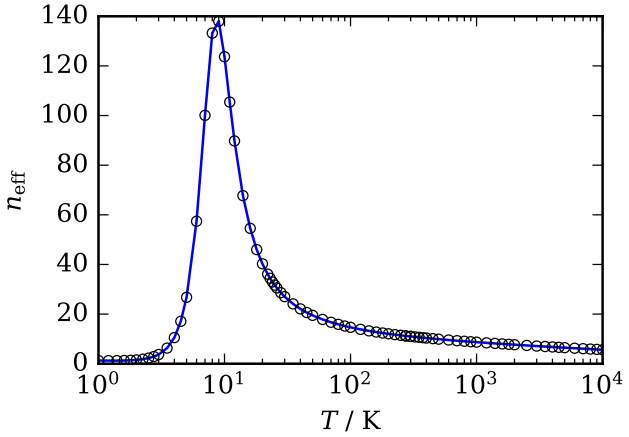

FIG. 8. Effective IPL exponent n_{eff} for ^{4}He from the ab initio calculations[56]. Markers indicate tabulated values and are connected with straight line segments to guide the eye.

Similarly, the results for the Tang-Toennies integration described above provide reliable values of n_{eff} for the other noble gases. Figure 9 shows the curves calculated for the noble gases over an extreme range in temperature, outside the range where the species are stable. Contrary to the Lennard-Jones potential (see for instance Fig. 3), the high temperature limit does not approach a horizontal asymptote in n_{eff} at high temperatures.

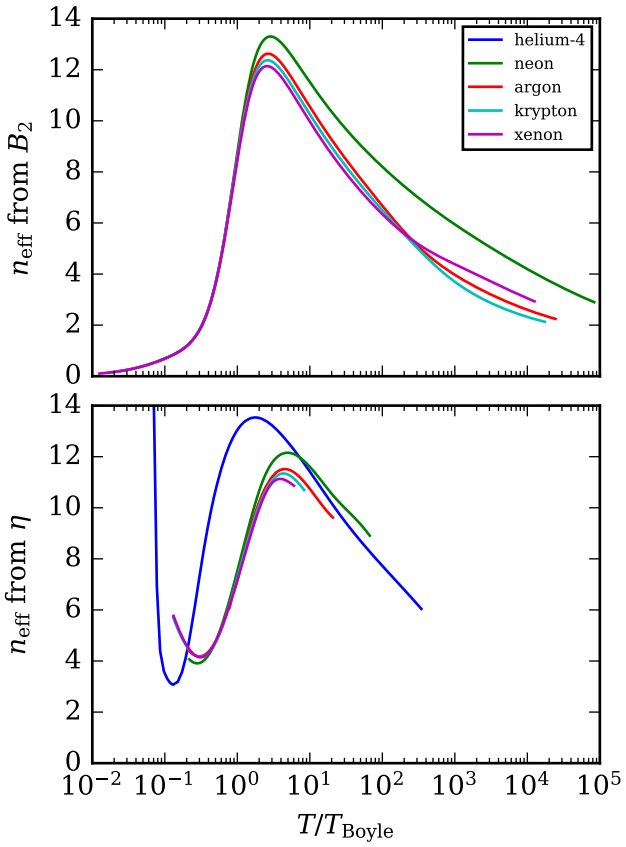

FIG. 9. Effective IPL exponent n_{eff} for the noble gases from B_2 (upper panel; helium-4 in Fig. 8) and η (lower panel) routes. Values for η taken from the literature (helium-4[56], neon[55], argon[46], krypton[47], xenon[53]).

3. Viscosity

For the ab initio data of shear viscosity, the effective collision integral for each discrete ab initio calculation is defined by

$$\widetilde{\Omega}_{22} = \frac{\sqrt{T}}{\eta}. \tag{53}$$

The values of η were taken from classical calculations presented in the literature for each species (helium-4[56], neon[55], argon[46], krypton[47], xenon[53]). There is some noise in the viscosity data, and as such, calculating the derivative of $\widetilde{\Omega}_{22}$ with respect to temperature requires some additional processing. To evaluate the derivative, moving windows of 5 points were fit by a third degree polynomial, and this approach yielded a noisy value for n_{eff}, which was then smoothed to decrease the noise. Some artifacts of the fitting approach can be identified, but the overall curves are mostly smooth.

Figure 9 also presents the effective IPL exponent obtained by this method. These results show that the effective IPL exponent obtained by the viscosity route is very similar to that of the thermodynamic route, in both quantitative and qualitative agreement. Both show a peak at approximately the same temperature, and have similar high-temperature limits as well. On the other hand, the low-temperature behavior differs. In the case of the effective hardness coming from viscosity, there is a local minimum at a value of n_{eff} of approximately 4. An extreme anomaly can be seen in the case of helium-4, for which its viscosity n_{eff} is similar to those of the heavier noble gases, while its thermodynamic n_{eff} is an order of magnitude higher at its peak (see Fig. 8).

B. Molecules

1. Rigid Lennard-Jones Chains

One of the present limitations of ab initio calculations is that they can only be carried out for quite small molecules. On the other hand, larger molecules are still of technical relevance. A fair question is whether the behavior seen here for small molecules should be expected to continue for larger molecules. One model system that can provide some insight into this question is rigid linear chains of Lennard-Jones 12-6 sites. This model, unphysical because it does not include intramolecular flexibility, can nonetheless provide some insight into the effective IPL exponent for larger molecules. For a potential with orientational dependence, the second virial coefficient is obtained from

$$B_2 = -2\pi N_{\text{A}} \int_0^\infty \left(\langle \exp(-\beta V)\rangle - 1\right) r^2 \mathrm{d}r, \tag{54}$$

where $\langle \exp(-\beta V)\rangle$ is the orientational average of the potential for a center-of-mass separation of r. The orientational average of a function $G(\theta_1, \theta_2, \phi)$ for a molecule with axial symmetry is defined generically by

$$\langle G\rangle = \frac{1}{8\pi} \int_0^{2\pi} \int_0^{\pi} \int_0^{\pi} G \sin\theta_1 \sin\theta_2 d\theta_1 d\theta_2 d\phi \tag{55}$$

with the normalization constant of 8π being obtained from the triple integral with the argument of $G \equiv 1$.

In order to evaluate $\exp(-\beta V)$ for a given set of (r, θ_1, θ_2, ϕ), the linear molecule was initialized with its center of mass at the origin of the Cartesian coordinate system, with its sites oriented along the x axis, and then one molecule was rotated around the $-y$ axis by the angle θ_1 (keeping the molecule in the x-z plane), and the second molecule was rotated around the $-y$ axis by the angle θ_2, around the $+x$ axis by the angle ϕ, and then translated in the $+x$ direction by r. The site-site interactions of each site i on the first molecule with each site j on the second molecule are summed, forming M^2 interactions for a chain with M beads. Figure 10 shows a schematic of the definition of the geometry of the molecules.

The code for the analysis used open-source thread-parallelized code written in modern C++ (https://github.com/usnistgov/potter) to carry out the integration for B_2 simultaneously with its temperature derivatives.

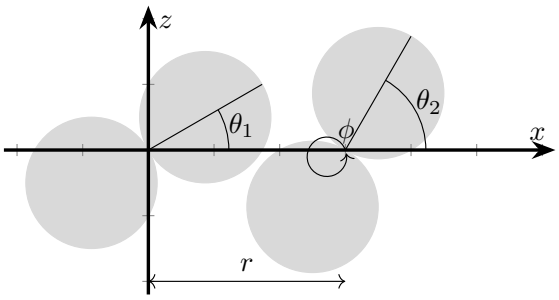

FIG. 10. Schematic showing the definitions of the angles θ_1, θ_2, and ϕ for dimers projected into the $x-z$ plane. The rotation angle ϕ is a rotation taken around the $+x$ axis.

This study represents the author's first experience with the calculation of second virial coefficients for rigid linear molecules, so verification was carried out, calculating second virial coefficients that agreed with the results for dimers[58–60]. Results for dimers with alternative potential truncation schemes can also be found in the literature[61,62]. Results verifying the classical second virial coefficients for nitrogen[63] are also provided in the code, showing that the approach agrees with the state-of-the-art calculations to nearly the error estimation from the Monte Carlo-sampled potential. Finally, results for the rigid 8-mer and 16-mer from Monte Carlo methods were calculated by another group with an independent code[64], along with their temperature derivatives, confirming the values obtained in this work.

Figure 11 shows the effective exponents calculated from the viscosity and thermodynamic routes for the rigid Lennard-Jones chains. In the case of the thermodynamic n_{eff}, the curves are still coherent with the simple potentials though there is a larger magnitude peak followed by a decay to the value of 12 in the infinite temperature limit. This asymptote implies that the high-temperature limit is governed by the site-site interactions at contact with the r^{-12} repulsion.

The magnitude of the values for the viscosity n_{eff} values are much larger. The curves tend to move upwards as the chain length increases, a trend also noted by Hellmann et al.[19]; their analysis considered the mean value of n_{eff} in the temperature range $5 < T^* < 50$, whereas the present study considers also the temperature dependence of the effective hardness, rather than just the mean. The hypothesis, not accessible with the present calculation data, is that n_{eff} for the longer chains would also reach a maximum at sufficiently high temperatures, followed by a decay back to the value of 12, in analogy to the values from the thermodynamic n_{eff} values. The discrepancy between values of n_{eff} can be attributed to the extreme anisotropy in the rigid Lennard-Jones chain model as compared to more physical models like fully flexible Lennard-Jones chains, which are more similar to real fluids (e.g., alkanes).

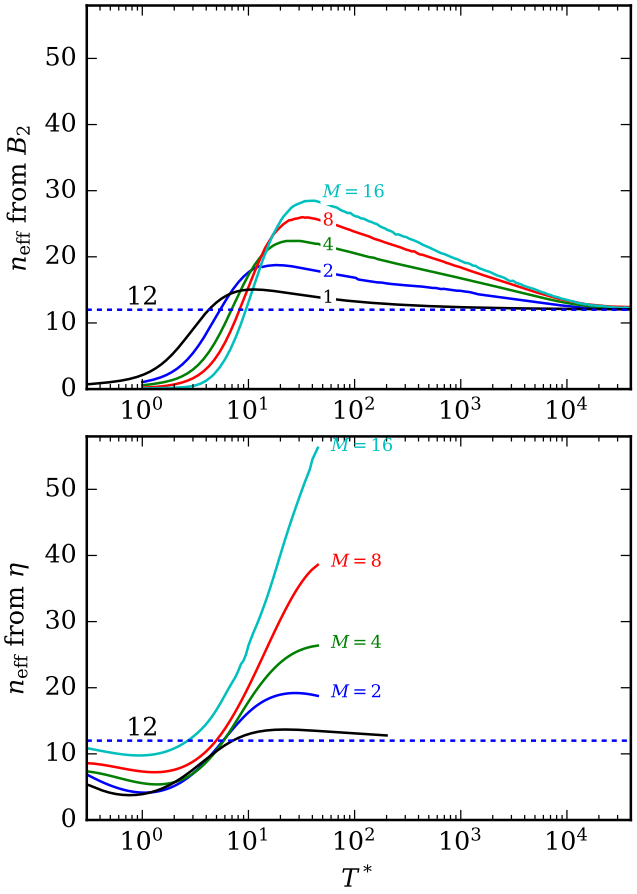

FIG. 11. Effective IPL exponent n_{eff} for rigid LJC chains of site-site distance σ and number of sites of 2,4,8,16 from the viscosity and B_2 routes. Viscosity data from Hellmann et al.[19]. A figure with additional chain lengths is in the SI, Figure **??**. The black curve indicates the monomer value.

Galliero et al.[65] found that the viscosity n_{eff} values varied from 14.7 for the monomer to 19.8 for the 16-mer for fully-flexible Lennard-Jones chains from dense-phase molecular dynamics. If the maximum values for the thermodynamic n_{eff} are used, and are overlaid with the averaged values taken from Hellmann's data for rigid chain viscosity (obtained from the slope of a linear fit of $\ln(\eta^*)$ versus $\ln(T^*)$ for $T^* > 5$), and Galliero's data for flexible chain viscosity, they all show that the averaged effective hardness is increasing as the chain length increases. This does not represent an apples-to-apples comparison, but nonetheless, all three methods yield a similar conclusion: the longer the chain, the more effectively repulsive the chains are, up to a point. At very high temperatures, the effective interaction is again controlled by site-site interactions.

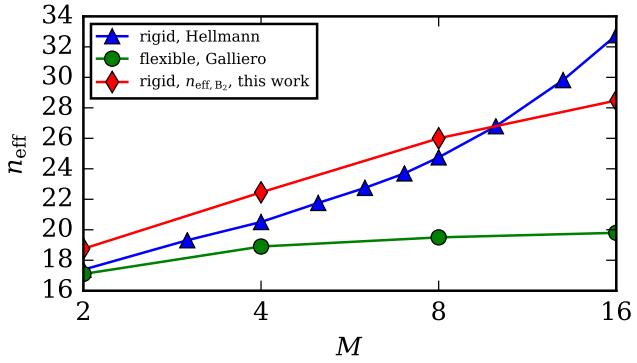

FIG. 12. Summary of n_{eff} values for rigid Lennard-Jones chains with M segments (obtained from this study and Hellmann et al.[19]) and for fully-flexible Lennard-Jones chains[65]. Note the logarithmic abscissa. Points are connected with lines to guide the eye.

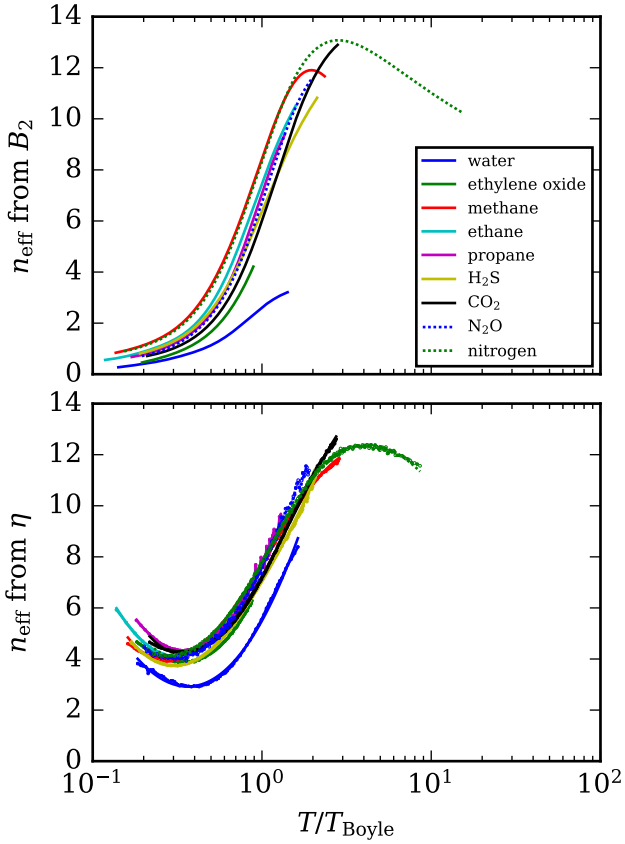

FIG. 13. Effective IPL exponent n_{eff} for polyatomic molecules via B_2 and η routes

2. *Polyatomic Molecules*

Obtaining the second (and higher) virial coefficients from integration of the potential between molecules (along with quantum corrections) is much more complicated for polyatomic molecules than for monatomic gases. As such, while in theory multifold integration over orientation and center-of-mass separation could be carried out to obtain the second virial coefficients, and multicomplex algebgra used to calculate the temperature derivatives (as above for the noble gases), a more pragmatic approach is taken here. While empirical fits of B_2 data from ab initio calculations are often infected by spurious changes in curvature, they are usually at least reasonable in their qualitative behavior.

The same fluids as in Ref. 30 were considered, except for heavy water, for which reasonable high temperature behavior of n_{eff} could not be achieved from empirical correlations of B_2. In the case of heavy water, the behavior of n_{eff} should be very similar to that of ordinary water, but it was not, and this difference was already present in the first derivative of B_2[30] (see Fig. 8). In the case of hydrogen sulfide, the published data[66] are calculated values from correlations of the data, and the underlying ab initio results were provided by the authors[67].

Figure 13 shows the values of n_{eff} obtained from the empirical models for B_2, and the curves are qualitatively similar to those of the noble gases. The temperature was normalized by the Boyle temperature (obtained from the fit of B_2, the temperature where $B_2 = 0$). The values for water are much lower, and do not follow the same trajectory as the other fluids studied here, which show a striking similarity.

The same approach as for the noble gases for n_{eff} coming from the viscosity data is used. The effective collision integral is defined by Eq. (53), and Eq. (17) is used to obtain the effective IPL exponent. Here too, the qualitative agreement is similar among all the fluids studied, with the exception of water, which is decidedly different. In fact, the effective hardness coming from the viscosity data is even more similar than those coming from the virial coefficients. The curves are nearly indistinguishable for many of the fluids.

V. PRACTICAL APPLICATIONS

The analysis thus far has been very theoretical in nature, investigating model systems and small rigid molecules. One of the practical ramifications of this work is that it shows that the high-temperature behavior of the n_{eff} coming from both thermodynamic and transport routes are generally similar. This has a tangible consequence: because the n_{eff} are approaching each other at high temperatures, both thermodynamics and transport should be governed by the same effective IPL exponent. Thus, the values of η^+ for real fluids should fall between 0.2580 ($n = 6$) and 0.2886 ($n = \infty$) in the high temperature limit, and should stay within this band. It is not clear that this behavior should *necessarily* hold for large flexible molecules

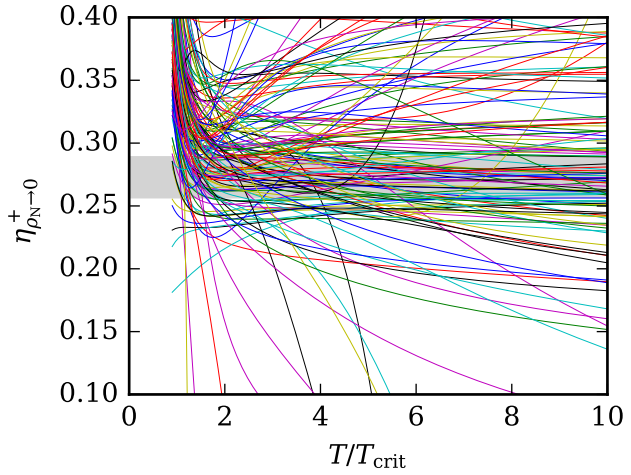

FIG. 14. Values of η^+ in the dilute-gas limit for the models in NIST REFPROP 10[68] as a function of reduced temperature; each curve represents one pure fluid. The grey band indicates the range of acceptable high-temperature values.

(e.g., proteins), but it seems likely that it would based on the discussion of the rigid Lennard-Jones chains.

The NIST REFPROP thermophysical property software is the de facto standard for the thermophysical properties of more than 150 of the most well measured chemical species and implements empirical correlations for thermodynamic and transport properties. Some of the selected models were implemented several decades ago, and our understanding of the appropriate behavior of these models has improved in the interim.

Figure 14 shows calculated values of η^+ up to extremes in temperature for the models implemented in NIST REFPROP version 10.0. The models for $\eta_{\rho_N\to 0}$ and B_2 are both invoked in order to calculate η^+, according to Eq. (35). Of the more than 140 fluids for which REFPROP provides viscosity models, only 22 yield predictions of η^+ that are within the acceptable band at a temperature of 10 times the critical temperature, a temperature at which most molecules are already ionized, or fully dissociated. The analysis in this work suggests that a consideration of n_{eff} for both of transport and viscosity can result in much more consistent thermodynamic and transport models at high temperatures.

VI. OUTLOOK AND RECOMMENDATIONS

The effective hardness is shown to behave in a similar fashion for both transport and thermodynamics, especially at high temperatures. Arriving from two different directions, the effective hardness can be expressed as -2 divided by the double-logarithmic derivative of an effective area with respect to the temperature (Eq. (14) and Eq. (17)). The identical mathematical form suggests a heretofore novel interpretation of the interplay between thermodynamics and molecular transport. It is speculated (though not yet confirmed) that the effective hardness represents a universal means of linking transport properties and thermodynamics, though the “proof" remains empirical in nature.

The approach proposed in this work brings quantitative constraints into the high-temperature extrapolation of the coupled transport and thermodynamic models in the dilute gas limit. The condition of η^+ being within the band of 0.25 to 0.29 in the limit of high temperatures is a very stringent test. As such, the transport and thermodynamic models need to be developed concurrently in order to ensure that the models will extrapolate correctly when coupled together.

The Boyle temperature can be thought of as the temperature at which the interactions between pairs of molecules transition from being attractive (on average) to repulsive (on average). The Boyle temperature is very roughly equal to 2.5 times the critical temperature[69]. Therefore, it is reasonable to expect that above the Boyle temperature, when combining the transport and thermodynamics models together, they should yield a value of η^+ like those of an IPL.

Discussing the properties of a fluid such as propane at 3600 K is of purely academic interest as such a fluid no longer exists at this temperature, but the appropriate extrapolation behavior of $\eta^+_{\rho_N\to 0}$ and B_2 at *extremely* high temperatures also ensures quantitatively correct extrapolation at more moderate temperatures of technical relevance but at which no experimental data may exist.

VII. SUPPLEMENTARY MATERIAL

In order to ensure reproducibility of our results, the supplementary material includes:

- The Python code and analysis for integration of the Tang-Toennies potentials with quantum corrections
- The Python code and analysis for the square-well fluid
- An archival copy of potter. The repository can be found at https://github.com/usnistgov/potter.
- The tabular results for the rigid Lennard-Jones chains
- Additional mathematical analysis and figures

ACKNOWLEDGMENTS

Thanks are given to Allan Harvey (of NIST) for assistance with integration of the Tang-Toennies potentials and generous brainstorming, Andrew Schultz (of University at Buffalo) for providing confirmatory calculations of B_2 for rigid n-mers, Robert Hellmann (of Helmut-Schmidt-Universität) for extensive discussion and providing the tabular data from publications, J. Richard Elliot (of University of Akron) for the inspiration to consider the square-well potential, and Marcia Huber (of NIST), for the recommendation to consider the Stockmayer fluid.

VIII. DATA AVAILABILITY

Data available in article, supplementary material, and linked code repository. For more detailed information, or additional clarifications, please contact the author.

[1] R. J. Munn, "Interaction Potential of the Inert Gases. I," J. Chem. Phys. **40**, 1439–1446 (1964).

[2] J. H. Dymond, M. Rigby, and E. B. Smith, "Intermolecular Potential-Energy Function for Simple Molecules," J. Chem. Phys. **42**, 2801–2806 (1965).

[3] F. J. Smith, E. A. Mason, and R. J. Munn, "Transport Collision Integrals for Gases Obeying 9–6 and 28–7 Potentials," J. Chem. Phys. **42**, 1334–1339 (1965).

[4] J. A. Barker, W. Fock, and F. Smith, "Calculation of Gas Transport Properties and the Interaction of Argon Atoms," Physics of Fluids **7**, 897 (1964).

[5] R. J. Munn and F. J. Smith, "Interaction potential of the inert gases. II," J. Chem. Phys. **43**, 3998–4002 (1965).

[6] D. D. Konowalow, "Central Potentials for Nonpolar Polyatomic Molecules," Physics of Fluids **9**, 23 (1966).

[7] L. S. Tee, S. Gotoh, and W. E. Stewart, "Molecular Parameters for Normal Fluids. Lennard-Jones 12-6 Potential," Ind. Eng. Chem. Fundam. **5**, 356–363 (1966).

[8] J. H. Dymond, "Two-Parameter Intermolecular Potential Energy Functions for Simple Molecules," Physics of Fluids **9**, 1222 (1966).

[9] N. S. Barlow, A. J. Schultz, S. J. Weinstein, and D. A. Kofke, "An asymptotically consistent approximant method with application to soft- and hard-sphere fluids," J. Chem. Phys. **137**, 204102 (2012).

[10] D. M. Heyes, G. Rickayzen, S. Pieprzyk, and A. C. Brańka, "The second virial coefficient and critical point behavior of the Mie Potential," J. Chem. Phys. **145**, 084505 (2016).

[11] J. C. Dyre, "Simple liquids' quasiuniversality and the hard-sphere paradigm," J. Phys.: Condens. Matter **28**, 323001 (2016).

[12] T. B. Schrøder, N. P. Bailey, U. R. Pedersen, N. Gnan, and J. C. Dyre, "Pressure-energy correlations in liquids. III. Statistical mechanics and thermodynamics of liquids with hidden scale invariance," J. Chem. Phys. **131**, 234503 (2009).

[13] T. B. Schrøder, N. Gnan, U. R. Pedersen, N. P. Bailey, and J. C. Dyre, "Pressure-energy correlations in liquids. V. Isomorphs in generalized Lennard-Jones systems," J. Chem. Phys. **134**, 164505 (2011).

[14] T. B. Schrøder and J. C. Dyre, "Simplicity of condensed matter at its core: Generic definition of a Roskilde-simple system," J. Chem. Phys. **141**, 204502 (2014).

[15] N. Gnan, T. B. Schrøder, U. R. Pedersen, N. P. Bailey, and J. C. Dyre, "Pressure-energy correlations in liquids. IV. "Isomorphs" in liquid phase diagrams," J. Chem. Phys. **131**, 234504 (2009).

[16] P. Mausbach, A. Köster, and J. Vrabec, "Liquid state isomorphism, Rosenfeld-Tarazona temperature scaling, and Riemannian thermodynamic geometry," Phys. Rev. E **97**, 052149 (2018).

[17] N. P. Bailey, L. Bøhling, A. A. Veldhorst, T. B. Schrøder, and J. C. Dyre, "Statistical mechanics of Roskilde liquids: Configurational adiabats, specific heat contours, and density dependence of the scaling exponent," J. Chem. Phys. **139**, 184506 (2013).

[18] I. H. Bell, R. Messerly, M. Thol, L. Costigliola, and J. Dyre, "Modified Entropy Scaling of the Transport Properties of the Lennard-Jones Fluid," J. Phys. Chem. B , 6345–6363 (2019).

[19] R. Hellmann, N. Riesco, and V. Vesovic, "Calculation of the transport properties of a dilute gas consisting of Lennard-Jones chains," J. Chem. Phys. **138**, 084309 (2013).

[20] J. C. Castro-Palacio, R. Hellmann, and V. Vesovic, "Dilute gas viscosity of n-alkanes represented by rigid Lennard-Jones chains," Mol. Phys. **114**, 3171–3182 (2016).

[21] E. A. Mason, "Transport Properties of Gases Obeying a Modified Buckingham (Exp-Six) Potential," J. Chem. Phys. **22**, 169–186 (1954).

[22] Y. Rosenfeld, "A quasi-universal scaling law for atomic transport in simple fluids," J. Phys.: Condens. Matter **11**, 5415–5427 (1999).

[23] I. H. Bell, "Probing the link between residual entropy and viscosity of molecular fluids and model potentials," Proc. Natl. Acad. Sci. U.S.A. **116**, 4070–4079 (2019).

[24] N. P. Bailey, U. R. Pedersen, N. Gnan, T. B. Schrøder, and J. C. Dyre, "Pressure-energy correlations in liquids. I. Results from computer simulations," J. Chem. Phys. **129**, 184507 (2008).

[25] N. P. Bailey, U. R. Pedersen, N. Gnan, T. B. Schrøder, and J. C. Dyre, "Pressure-energy correlations in liquids. II. Analysis and consequences," J. Chem. Phys. **129**, 184508 (2008).

[26] J. C. Dyre, "Perspective: Excess-entropy scaling," J. Chem. Phys. **149**, 210901 (2018).

[27] J. C. Dyre, "Isomorphs, hidden scale invariance, and quasiuniversality," Phys. Rev. E **88**, 042139 (2013).

[28] T. S. Ingebrigtsen, T. B. Schrøder, and J. C. Dyre, "Isomorphs in Model Molecular Liquids," J. Phys. Chem. B **116**, 1018–1034 (2012).

[29] A. E. Olsen, J. C. Dyre, and T. B. Schrøder, "Communication: Pseudoisomorphs in liquids with intramolecular degrees of freedom," J. Chem. Phys. **145**, 241103 (2016).

[30] I. H. Bell, R. Hellmann, and A. H. Harvey, "Zero-Density Limit of the Residual Entropy Scaling of Transport Properties," J. Chem. Eng. Data (2019), 10.1021/acs.jced.9b00455.

[31] J. D. Weeks, D. Chandler, and H. C. Andersen, "Role of Repulsive Forces in Determining the Equilibrium Structure of Simple Liquids," J. Chem. Phys. **54**, 5237–5247 (1971).

[32] J. A. Barker and D. Henderson, "Perturbation Theory and Equation of State for Fluids. II. A Successful Theory of Liquids," J. Chem. Phys. **47**, 4714–4721 (1967).

[33] J. E. Jones, "On the Determination of Molecular Fields. II. From the Equation of State of a Gas," Proc. R. Soc. London, Ser. A **106**, 463–477 (1924).

[34] R. J. Sadus, "Second virial coefficient properties of the n-m Lennard-Jones/Mie potential," J. Chem. Phys. **149**, 074504 (2018).

[35] R. J. Sadus, "Erratum: "Second virial coefficient properties of the n-m Lennard-Jones/Mie potential" [J. Chem. Phys. 149, 074504 (2018)]," J. Chem. Phys. **150**, 079902 (2019).

[36] S. U. Kim and C. W. Monroe, "High-accuracy calculations of sixteen collision integrals for Lennard-Jones (12–6) gases and their interpolation to parameterize neon, argon, and krypton," J. Comput. Phys. **273**, 358–373 (2014).

[37] A. E. Sherwood and E. A. Mason, "Virial Coefficients for the Exponential Repulsive Potential," Phys. Fluids **8**, 1577–1579 (1965).

[38] J. Kestin, K. Knierim, E. A. Mason, B. Najafi, S. T. Ro, and M. Waldman, "Equilibrium and Transport Properties of the Noble Gases and Their Mixtures at Low Density," J. Phys. Chem. Ref. Data **13**, 229–303 (1984).

[39] L. Monchick, "Collision Integrals for the Exponential Repulsive Potential," Phys. Fluids **2**, 695–700 (1959).

[40] H. W. Xiang, A. Laesecke, and M. L. Huber, "A New Reference Correlation for the Viscosity of Methanol," J. Phys. Chem. Ref. Data **35**, 1597–1620 (2006).

[41] J. Bartke and R. Hentschke, "Phase behavior of the Stockmayer fluid via molecular dynamics simulation," Phys. Rev. E **75**, 061503 (2007).

[42] I. H. Bell, "mcx: A library for working with multicomplex algebra," (2019).

[43] J. O. Hirschfelder, C. F. Curtiss, and R. B. Bird, *Molecular Theory of Gases and Liquids* (John Wiley and Sons, 1954).

[44] L. Monchick and E. A. Mason, "Transport Properties of Polar Gases," J. Chem. Phys. **35**, 1676–1697 (1961).

[45] F. J. Smith and R. J. Munn, "Automatic Calculation of the Transport Collision Integrals with Tables for the Morse Potential," J. Chem. Phys. **41**, 3560–3568 (1964).

[46] E. Vogel, B. Jäger, R. Hellmann, and E. Bich, "Ab initio pair potential energy curve for the argon atom pair and thermophysical properties for the dilute argon gas. II. Thermophysical properties for low-density argon," Mol. Phys. **108**, 3335–3352 (2010).

[47] B. Jäger, R. Hellmann, E. Bich, and E. Vogel, "State-of-the-art ab initio potential energy curve for the krypton atom pair and thermophysical properties of dilute krypton gas," J. Chem. Phys. **144**, 114304 (2016).

[48] J. C. Slater, "The Normal State of Helium," Phys. Rev. **32**, 349–360 (1928).

[49] U. K. Deiters and R. J. Sadus, "Two-body interatomic potentials for He, Ne, Ar, Kr, and Xe from ab initio data," J. Chem. Phys. **150**, 134504 (2019).

[50] M. Przybytek, W. Cencek, J. Komasa, G. Łach, B. Jeziorski, and K. Szalewicz, "Relativistic and Quantum Electrodynamics Effects in the Helium Pair Potential," Phys. Rev. Lett. **104** (2010), 10.1103/PhysRevLett.104.183003.

[51]R. Hellmann, E. Bich, and E. Vogel, "Ab initio potential energy curve for the neon atom pair and thermophysical properties of the dilute neon gas. I. Neon–neon interatomic potential and rovibrational spectra," Mol. Phys. **106**, 133–140 (2008).
[52]B. Jäger, R. Hellmann, E. Bich, and E. Vogel, "Ab initio pair potential energy curve for the argon atom pair and thermophysical properties of the dilute argon gas. I. Argon–argon interatomic potential and rovibrational spectra," Mol. Phys. **107**, 2181–2188 (2009).
[53]R. Hellmann, B. Jäger, and E. Bich, "State-of-the-art ab initio potential energy curve for the xenon atom pair and related spectroscopic and thermophysical properties," J. Chem. Phys. **147**, 034304 (2017).
[54]E. Bich, R. Hellmann, and E. Vogel, "Ab initio potential energy curve for the neon atom pair and thermophysical properties for the dilute neon gas. II. Thermophysical properties for low-density neon," Mol. Phys. **106**, 813–825 (2008).
[55]E. Bich, R. Hellmann, and E. Vogel, "Erratum to : "Ab initio potential energy curve for the neon atom pair and thermophysical properties for the dilute neon gas. II. Thermophysical properties for low-density neon"," Mol. Phys. **106**, 1107–1122 (2008).
[56]W. Cencek, M. Przybytek, J. Komasa, J. B. Mehl, B. Jeziorski, and K. Szalewicz, "Effects of adiabatic, relativistic, and quantum electrodynamics interactions on the pair potential and thermophysical properties of helium," J. Chem. Phys. **136**, 224303 (2012).
[57]M. Przybytek, W. Cencek, B. Jeziorski, and K. Szalewicz, "Pair Potential with Submillikelvin Uncertainties and Nonadiabatic Treatment of the Halo State of the Helium Dimer," Phys. Rev. Lett. **119** (2017), 10.1103/physrevlett.119.123401.
[58]T. Boublík, "Second Virial Coefficient of the 2cLJ, 3cLJ and 4cLJ Molecules," Collect. Czech. Chem. Commun. **59**, 756–767 (1994).
[59]C. Vega, C. McBride, and C. Menduiña, "The second virial coefficient of the dipolar two center Lennard-Jones model," Phys. Chem. Chem. Phys. **4**, 3000–3007 (2002).
[60]Y. Chiew and V. Sabesan, "Second virial coefficients of Lennard–Jones chains," Fluid Phase Equilib. **155**, 75–83 (1999).
[61]V. I. Harismiadis and I. Szleifer, "Second virial coefficients of chain molecules: A Monte Carlo study," Mol. Phys. **81**, 851–866 (1994).
[62]I. M. Withers, A. V. Dobrynin, M. L. Berkowitz, and M. Rubinstein, "Monte Carlo simulation of homopolymer chains. I. Second virial coefficient," J. Chem. Phys. **118**, 4721–4732 (2003).
[63]R. Hellmann, "Ab initio potential energy surface for the nitrogen molecule pair and thermophysical properties of nitrogen gas," Mol. Phys. **111**, 387–401 (2013).
[64]A. Schultz, "Personal communication with Andrew Schultz, University at Buffalo (January 10, 2020),".
[65]G. Galliero, C. Boned, and J. Fernández, "Scaling of the viscosity of the Lennard-Jones chain fluid model, argon, and some normal alkanes," J. Chem. Phys. **134**, 064505 (2011).
[66]R. Hellmann, E. Bich, E. Vogel, and V. Vesovic, "Thermophysical Properties of Dilute Hydrogen Sulfide Gas," J. Chem. Eng. Data **57**, 1312–1317 (2012).
[67]R. Hellmann, "Personal communication with Robert Hellmann, Helmut-Schmidt-Universität (December 11, 2019),".
[68]E. W. Lemmon, I. H. Bell, M. L. Huber, and M. O. McLinden, "NIST Standard Reference Database 23: Reference Fluid Thermodynamic and Transport Properties-REFPROP, Version 10.0, National Institute of Standards and Technology," http://www.nist.gov/srd/nist23.cfm (2018).
[69]R. Estrada-Torres, G. A. Iglesias-Silva, M. Ramos-Estrada, and K. R. Hall, "Boyle temperatures for pure substances," Fluid Phase Equilib. **258**, 148–154 (2007).